Chapter 4

Modeling Implant Damage Enhanced Diffusion Using SUPREM-IV

4.1 Introduction

In Chapter 3, experimental data characterizing the effect of silicon implant damage on the diffusion of a buried boron marker layer was presented. The effect of silicon implant dose, silicon implant energy, anneal time, and anneal temperature were all investigated.

In this chapter, the ability of SUPREM-IV to model these results is discussed in detail. In particular we focus on the time and temperature dependence. First, we investigate whether or not an exponential decay can be used to describe the time dependence of IED. Second, the different diffusion models in SUPREM-IV are presented, and the models which can be applied to IED are pointed out. Third, the choice of the initial point defect profile to use in the simulation of IED is discussed. Fourth, two recent models proposed to account for IED are reviewed, and we show the inability to simulate the experimental data using either model. Finally, for our experimental data, we show that a two time transition model is necessary. We propose that the first transient in the enhanced diffusion is due to the decay of an initial interstitial excess due to the damage implant and that the second transient is due to the long-time dissolution of interstitial-type clusters. Using SUPREM-IV, the ability to model the two time transitions at 750˚C is shown. An initial scaled +1 interstitial profile can generate the short-time transition while a modified version of the dislocation loop model presented in Section 2.2.5 can generate the long-time transition by mimicking the dissolution of very small interstitial-type clusters.

4.2 Exponential Solution

We first investigate whether the transient-enhanced diffusion data from Chapter 3 can be modeled using a simple analytic exponential decay which is the solution to a first order reaction. If an independent interstitial sink is the dominant recombination mechanism for excess interstitials, then one can drop all the other terms in the interstitial continuity equation producing the following differential equation:

$$\frac{\partial C_I}{\partial t} = -k\,(C_I - C_I^*) \tag{4.1}$$

The time-dependent solution to this equation is an exponential decay. Since boron diffuses mainly via an interstitial mechanism, then the diffusivity of boron would also follow an exponential decay. Throughout this chapter the $4\text{x}10^{15}$ cm^{-2}, 50 keV silicon implanted samples annealed at 750ßC for 2, 10, 30, and 120 minutes (Figure 3.8) are assumed to be representative of the time-dependence of IED. In order to extract the best-fit exponential decay for boron diffusivity, rather than using the time-averaged enhancements referenced to the initial boron profile, we use the time-averaged enhancements between data points, i.e. the time-averaged enhancements from 0 to 2 minutes, from 2 to 10 minutes, from 10 to 30 minutes, and from 30 to 120 minutes. In Figure 4.1, solid lines are used to indicate that over a particular time interval, the enhancement in diffusivity is assumed constant. For curve-fitting purposes, only the values at the center of each time interval are used (solid symbols in the figure). Ignoring the 2 minute data point which is actually a 745ßC RTA, the best-fit exponential decay is found to be $<D>/D^*=2.55\text{x}10^2\text{exp}(-0.0374t)$ where t is the anneal time in minutes. This equation is indicated by the dotted line in the figure. An equivalent $<D>/D^*$ with respect to the initial profile was calculated for each time point by integrating the equation from time=0 up to the anneal time then dividing by the anneal

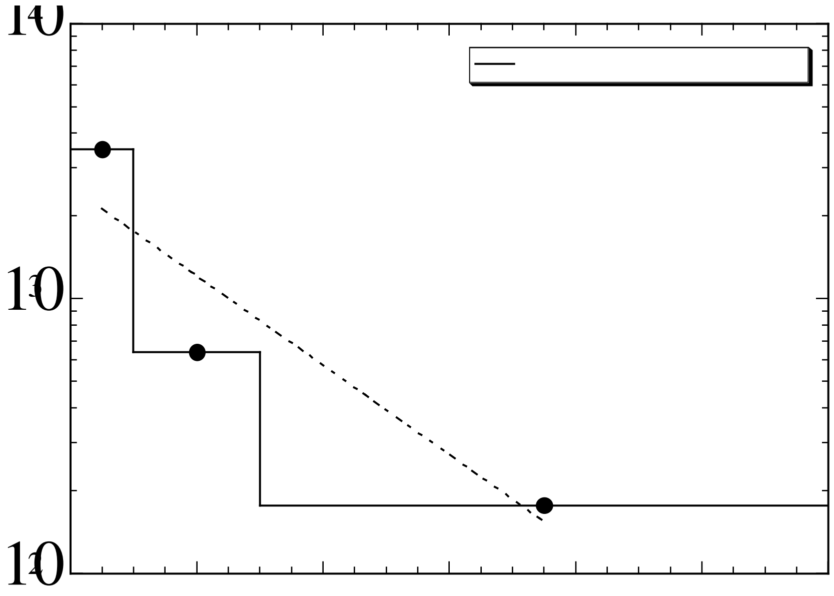

PostScript error

Figure 4.1 Time-averaged enhancements between time points for the $4x10^{15}$ cm^{-2}, 50 keV silicon implanted samples annealed at 750ßC for 10, 30, and 120 minutes. The best-fit exponential decay is represented by the dotted line and the parameters are given in the plot.

time. These enhancements were then used to generate the profiles in Figure 4.2. Although the fits to the 30 and 120 minute profiles are quite good, there is not enough motion in the 10 minute profile as compared to the SIMS data. If the 2 minute RTA is included, then one sees that the fits to short times are poor, and that the transient enhanced diffusion cannot be characterized by a simple exponential decay.

The actual time dependence of the enhanced diffusion will be a complex function of diffusion and recombination mechanisms for the point defects. In the rest of this chapter, more accurate numerical solutions which include these effects are evaluated to see whether or not the time-dependence of IED can be modeled. SUPREM-IV is used to perform the numerical simulations, and in the next section, the diffusion models in SUPREM-IV are described.

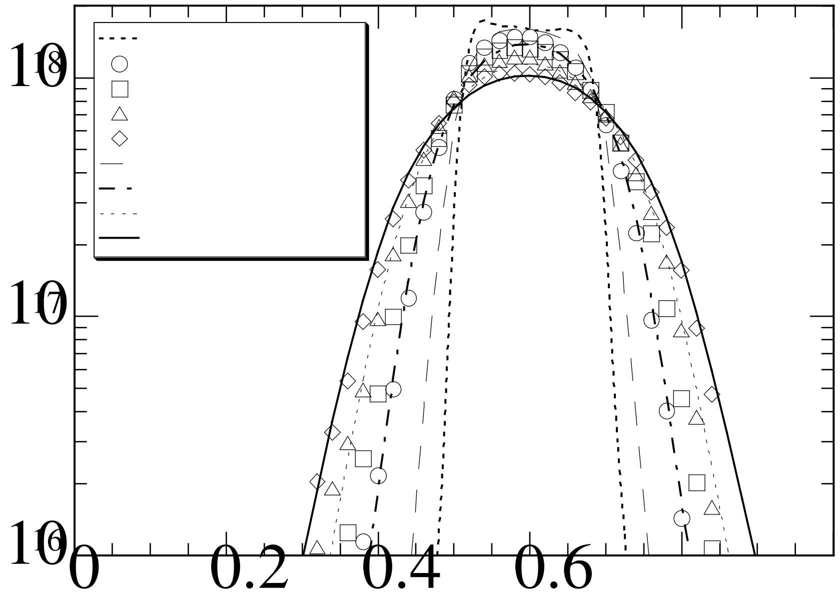

Figure 4.2 Comparison of best-fit exponential decay in the enhanced boron diffusion to the 10, 30, and 120 minute SIMS data.

PostScript error

4.3 Diffusion Models in SUPREM-IV

4.3.1 Fermi Model

The Fermi model is the simplest of the four diffusion models in SUPREM-IV. The Fermi model is Fick's Second Law including electric field effects. For p-type dopants:

$$\frac{\partial C_A}{\partial t} = \nabla \bullet \left[D_A C_A \nabla ln \left(C_A \frac{p}{n_i} \right) \right] \tag{4.2}$$

C_A is the dopant concentration, D_A is the dopant diffusivity, p is the hole concentration, and n_i is the intrinsic carrier concentration. For n-type dopants, p in Eq. 4.2 is replaced by n, the electron concentration.

This model can account for concentration-dependent diffusion since the diffusion constant is assumed to be a function of the Fermi level. In general,

$$D_A = D_A^0 + D_A^+ \left(\frac{p}{n_i}\right) + D_A^{++} \left(\frac{p}{n_i}\right)^2 + D_A^- \left(\frac{n}{n_i}\right) + D_A^{--} \left(\frac{n}{n_i}\right)^2 \tag{4.3}$$

D_A^0, D_A^+, D_A^{++}, D_A^-, and D_A^{--} account for the diffusion of the dopant with neutral, singly positively charged, doubly positively charged, singly negatively charged, and doubly negatively charged point defects, respectively. For p-type dopants, the neutral, singly positively charged and doubly positively charged components are dominant while for n-type dopants, the neutral, singly negatively charged, and doubly negatively charged components are dominant.

Without additional terms in the continuity equation or modifications to the diffusion coefficient, the Fermi model cannot be used to simulate nonequilibrium effects such as oxidation-enhanced diffusion (OED), nitridation-enhanced diffusion (NED), or implant-damage enhanced diffusion (IED) in which interstitials and/or vacancy concentrations are perturbed from their equilibrium values. In order to simulate these effects, one must use either the two.dim model or the full.cpl model described in Section 4.3.3 and Section 4.3.4, respectively.

4.3.2 Steady Model

In the steady model, the defect concentrations are assumed to be in steady-state. Since IED has previously been shown to be a transient effect, a steady-state model is not sufficient, and it is only mentioned here for completeness and is not discussed further.

4.3.3 Two.Dim Model

In the two.dim model, dopant diffusion is solved by using the dual defect model. At each numerical time step, the interstitial and vacancy concentrations are determined by solving the following continuity equations:

$$\frac{\partial C_I}{\partial t} = \nabla \bullet (D_I \nabla C_I) - K_R (C_I C_V - C_I^* C_V^*) \tag{4.4}$$

$$\frac{\partial C_V}{\partial t} = \nabla \bullet (D_V \nabla C_V) - K_R (C_I C_V - C_I^* C_V^*) \tag{4.5}$$

where the variables are defined as follows:

C_I: interstitial concentration
D_I: interstitial diffusivity
C_I^*: equilibrium interstitial concentration
K_R: bulk recombination coefficient
C_V: vacancy concentration
D_V: vacancy diffusivity
C_V^*: equilibrium vacancy concentration.

The interstitial and vacancy concentrations are subject to the following boundary conditions:

$$J_I \bullet \boldsymbol{n} + k_s^I (C_I - C_I^*) = g_I \tag{4.6}$$

$$J_V \bullet \boldsymbol{n} + k_s^V (C_V - C_V^*) = g_v \tag{4.7}$$

where J_I and J_V are the interstitital and vacancy fluxes, respectively, **n** is the surface normal, k_s^I and k_s^V are the interstitial and vacancy surface recombination coefficients, respectively, and g_I and g_v represent any surface interstitial and vacancy generation, respectively.

Once the solutions to the defect concentrations are obtained, the dopant concentrations are solved using:

$$\frac{\partial C_A}{\partial t} = \nabla \bullet \left[\left(D_{AI} \frac{C_I}{C_I^*} \frac{p}{n_i} \right) \nabla\, ln \left(C_A \frac{C_I}{C_I^*} \frac{p}{n_i} \right) + \left(D_{AV} \frac{C_V}{C_V^*} \frac{p}{n_i} \right) \nabla\, ln \left(C_A \frac{C_V}{C_V^*} \frac{p}{n_i} \right) \right] = -\nabla \bullet (J_{AI} + J_{AV}) \tag{4.8}$$

where D_{AI} and D_{AV} represent the interstitial and vacancy components of the dopant diffusivity, respectively, and J_{AI} and J_{AV} represent interstitial/dopant and vacancy/dopant fluxes, respectively. Again, for n-type dopants, the hole concentrations in Eq. 4.8 are replaced by electron concentration. The diffusivities are given by:

$$D_{AI} = f_I D_A \tag{4.9}$$

and

$$D_{AV} = (1 - f_I) D_A \tag{4.10}$$

where f_I is the fractional interstitial component of diffusivity which varies between 0 and 1, and D_A is the dopant diffusivity given by Eq. 4.3. A value of f_I equal to 1 means that particular dopant diffuses exclusively with interstitials while a value of f_I equal to 0 means that dopant diffuses entirely via a vacancy mechanism. Table 4.1 lists current f_I values for the common dopants in silicon. Boron and phosphorus diffuse predominantly with interstitials [12],[65], antimony diffuses predominantly with vacancies [66], and arsenic diffuses approximately half with interstitials and half with vacancies [66].

Dopant	f_I value	Reference
Phosphorus	1	Fahey *et al.* [65]
Boron	0.8	Packan and Plummer [12]
Arsenic	0.45-0.52	Perozziello *et al.* [66]
Antimony	< 0.03	Perozziello *et al.* [66]

Table 4.1 Common dopants in silicon along with their fractional interstitial components of diffusion.

These two.dim model equations reduce to the Fermi model if the defect concentrations are at equilibrium throughout the simulation. However, if the interstitial and/or vacancy concentrations are forced out of equilibrium, by surface injection or implant damage, for example, the two.dim equations can be used to simulate the subsequent effect on dopant diffusion.

4.3.4 Full.Cpl Model

The full.cpl model is the most advanced diffusion model in SUPREM-IV and is based on the work of Mathiot and Pfister [67]. The defect equations are:

$$\frac{\partial C_I}{\partial t} + \frac{\partial}{\partial t}\sum_{A,c} k_{AI^c} C_A C_{I^c} = \nabla \bullet \left(D_I \nabla C_I - \sum_A J_{AI}\right) - K_R\left(C_I C_V - C_I^* C_V^*\right) \tag{4.11}$$

and

$$\frac{\partial C_V}{\partial t} + \frac{\partial}{\partial t}\sum_{A,c} k_{AV^c} C_A C_{V^c} = \nabla \bullet \left(D_V \nabla C_V - \sum_A J_{AV}\right) - K_R\left(C_I C_V - C_I^* C_V^*\right) \tag{4.12}$$

The summations on the left-hand sides of the equals signs in Eq. 4.11 and Eq. 4.12 represent the paired defect/dopant species summed for all dopants, A, and for all defect charge states, c. The summations on the right-hand sides of the equals signs represent the corresponding dopant fluxes as defined by Eq. 4.8. In the full.cpl model, the dopant continuity equation remains the same as Eq. 4.8.

This formulation of the defect equations is important when the magnitudes of the dopant fluxes are comparable to the defect fluxes. This is exactly the case for high concentration phosphorus diffusion which exhibits a characteristic kink-and-tail profile. Dunham [68],[69] has recently used the full.cpl model to simulate high concentration phosphorus diffusion over a large range of anneal temperatures and surface concentrations. The full.cpl model, being a superset of the two.dim model, can also be used to simulate the effect of implant damage on dopant diffusion.

The emphasis of this thesis is the application of the two.dim and full.cpl models to IED. The descriptions of the diffusion models in SUPREM-IV given here are cursory presenting only the basic equations. For additional details, the reader is referred to references [7] and [70].

4.4 Initial Point Defect Profiles

Now that the constituent equations have been presented, the next issue of importance is the initial point defect profiles. Ion implantation generates many types of crystal damage in the implanted substrate. Jones *et al.* [8] have done extensive characterization of implant damage in silicon using both cross-sectional and plan-view TEM. They have classified the implant damage into five categories depending on the conditions of the implant. In this thesis, we focus on the generation of point defects, particularly interstitials, since boron diffuses primarily via an interstitial mechanism. Enhanced diffusion of boron persists until the interstitial concentration returns to its equilibrium value via diffusion and recombination mechanisms.

In ion implantation, atomic particles of a selected mass are accelerated towards a target sample. The implanted ions lose energy via two processes, elastic nuclear collisions and inelastic interaction with the potential field of the target sample. Initially, most of the incoming ions lose energy to the lattice of the crystal and slow down. As the ions lose more and more kinetic energy, the probability that they undergo a nuclear collision increases. In these nuclear events, the host atoms of the target sample are displaced. If a host atom travels far enough away from its original lattice site, then an interstitial/vacancy pair, also called a Frenkel pair, will have formed. The knocked on interstitial atoms acquire kinetic energy during collisions and can themselves create additional Frenkel pairs. Thus, the nuclear collisions are the main source of implantation damage as many interstitials and vacancies can be created due to the implantation of one ion.

In addition to the generation of Frenkel pairs, each implanted ion eventually becomes substitutional. Assuming no loss of mass, there is an additional interstitial profile that is exactly the same as the as-implanted profile which, unlike the Frenkel pairs, has no corresponding vacancy profile. Throughout the rest of this chapter, this initial interstitial profile will be referred to as the $+1$ profile.

If point defects and their concentrations could be directly measured, these would be the best initial defect profiles to use in SUPREM-IV simulations of IED. Unfortunately, there are currently no practical experimental methods which can measure interstitials or vacancies. For this reason, we rely on numerical simulations of ion implantation for the initial defect profiles.

Figure 4.3 shows a simulation result of a $1\text{x}10^{14}$ cm^{-2}, 80 keV silicon implant using a Boltzmann Transport Equation (BTE) solver [27],[28]. The Frenkel pairs, the net interstitial, the net vacancy, and the +1 profile are shown. The net interstitial and vacancy profiles are generated by subtracting the Frenkel pair profiles from each other. In qualitative agreement with Monte Carlo simulations of ion implantation [71], these net

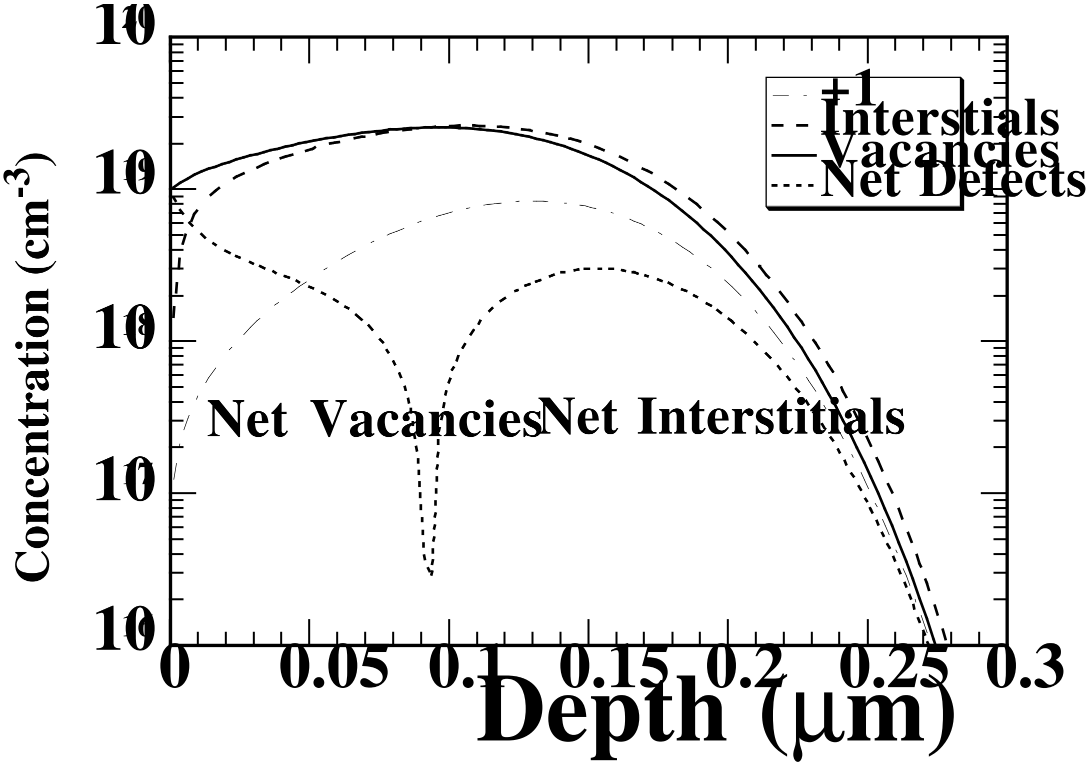

Figure 4.3 BTE simulation of a 1x10^{14} cm^{-2}, 80 keV silicon implant showing the intersititial and vacancy Frenkel pairs created as well as the as-implanted +1 profile.

profiles indicate that excess vacancies exist at the sample surface while excess interstitials exist deeper in the substrate. Physically, this is reasonable since one expects the knocked on atoms to end up slightly deeper than their original lattice positions. Crystal X-ray diffraction studies of substrates implanted below the amorphization threshold show only a surface region of positive strain which is correlated to the excess interstitial profile [45],[49]. The authors claim that the excess vacancies were not detected using this technique because vacancies create a weaker strain field than interstitials. However, it should be pointed out that samples implanted above the amorphization threshold and subsequently annealed to regrow the amorphous region do show a surface region of negative strain and a deeper region of positive strain [44]. In this case, the negative and positive lattice strains are attributed to vacancy-rich and interstitial-rich regions, respectively.

Giles [2] has investigated the sensitivity of SUPREM-IV simulations of subamorphizing IED to the initial defect profiles used. He simulated the IED of phosphorus using two different initial conditions. In the first simulation, the total Frenkel pairs and the +1 interstitial profile were used while in the second simulation, only the +1 profile was used. The simulated phosphorus diffusion during an 800ßC anneal was identical for the two cases. The reason for this behavior is that the large interstitial/vacancy pairs that are generated are separated by small distances such that most of these Frenkel defects annihilate each other very quickly via bulk recombination leaving behind the net interstitial and vacancy profiles. Except for the surface region, it is apparent from Figure 4.3 that the +1 profile is larger than either of the net defect profiles. Since phosphorus diffuses solely via an interstitial mechanism, the +1 interstitial profile dominates and controls phosphorus diffusion. Since boron diffuses mostly via an interstitial mechanism, we expect the +1 profile will also dominate boron diffusion after ion implantation. In contrast, arsenic and antimony have significant vacancy components of diffusion, and it may be important to include the net vacancy profile when simulating their diffusion after implantation.

Since the exact point defect profiles after ion implantation cannot be measured or calculated reliably at this time, since Giles has shown that a simulation of phosphorus IED using the +1 profile alone is indistinguishable from a simulation using the +1 profile and the Frenkel pairs, and since boron diffuses predominantly with interstitials, we have chosen to use the simple +1 approach in which the initial interstitial profile is the as-implanted profile. This is a reasonable first-order approximation until more accurate knowledge of the initial defects profiles can be obtained. For the remainder of the simulations presented in this thesis, the initial +1 profiles are calculated using the BTE method [27],[28].

Other than limiting the beam current to 300 µA, no other steps were taken to control the wafer temperature during our silicon implants. It is possible that the initial defect profile may be different for each wafer since implantation damage can vary with implant conditions. This is especially true for wafers implanted with different doses and energies and for wafers implanted at different times. In order to account for possible variations in the implant conditions, we introduce the scaled +1 approach. In this approach the +1 interstitial profile is scaled up or down by constant multiplicative factors. This liberty in scaling the +1 profile reflects the uncertainty in the initial defect profile. Again, similar to the +1 approach, the scaled +1 approach is a reasonable and simple approximation introduced to account for possible variations in implant conditions until a technique to measure point defect concentrations emerges.

4.5 Previous Models for IED

The basic equations and the initial defect concentration which will be used to model IED have now been defined. In this section two recent models that have been applied to low-dose IED are reviewed. The two models are used in an attempt to fit our $4x10^{15}$ cm^{-2}, 50 keV silicon implanted samples annealed at 750ßC for 2, 10, 30, and 120 minutes (Figure 3.8) and 800ßC for 5, 10, and 30 minutes (Figure 3.9) from Chapter 3. In fact, the 2 minute annealed sample is actually the 745ßC, 2 minute RTA annealed sample. All the rest of the samples were furnace annealed. This data set is assumed to be representative of the time and temperature dependence of moderate to high-dose IED.

4.5.1 Packan Model

Packan s model [11] is the two.dim model with the addition of one parameter, C_I^{max}, substituted for C_I in the dopant continuity equation (Eq. 4.8) when C_I is greater than C_I^{max}. Packan introduced this parameter in order to limit the maximum enhancement in dopant diffusivity to C_I^{max}/C_I^*. The reason for this was twofold. First, Packan used the full +1 profile for the initial interstitial concentration. When the full +1 profile is used with the two.dim model, extremely large interstitial supersaturations result in enhanced boron diffusion that is much larger than what was experimentally observed [1]. Second, as described in Section 3.2.1.3, for short anneal times, Packan observed a saturation in the enhanced diffusion as higher and higher damage doses were used. By capping the maximum interstitial supersaturation that can enhance dopant diffusion, Packan was able to simulate both of these effects.

Griffin *et al.* [23] have simulated both OED and low-dose IED using Packan s model and the parameter set given in Table 2.2 on page 27. This parameter set will be used as a starting point for our simulation of high-dose IED. In order to accurately simulate the enhanced diffusion for the 2 minute RTA sample, C_I^{max} has to be increased from the value in [23] to 15,025. However, if the full $4x10^{15}$ cm^{-2} +1 profile is used, only the 2 minute simulation agrees with the SIMS data. Too much enhanced diffusion occurs for longer times as compared to the experimental data (Figure 4.4). As previously discussed [30], the only way to simulate our high-dose IED data using Packan s model requires C_I^{max} to decrease as a function of time.

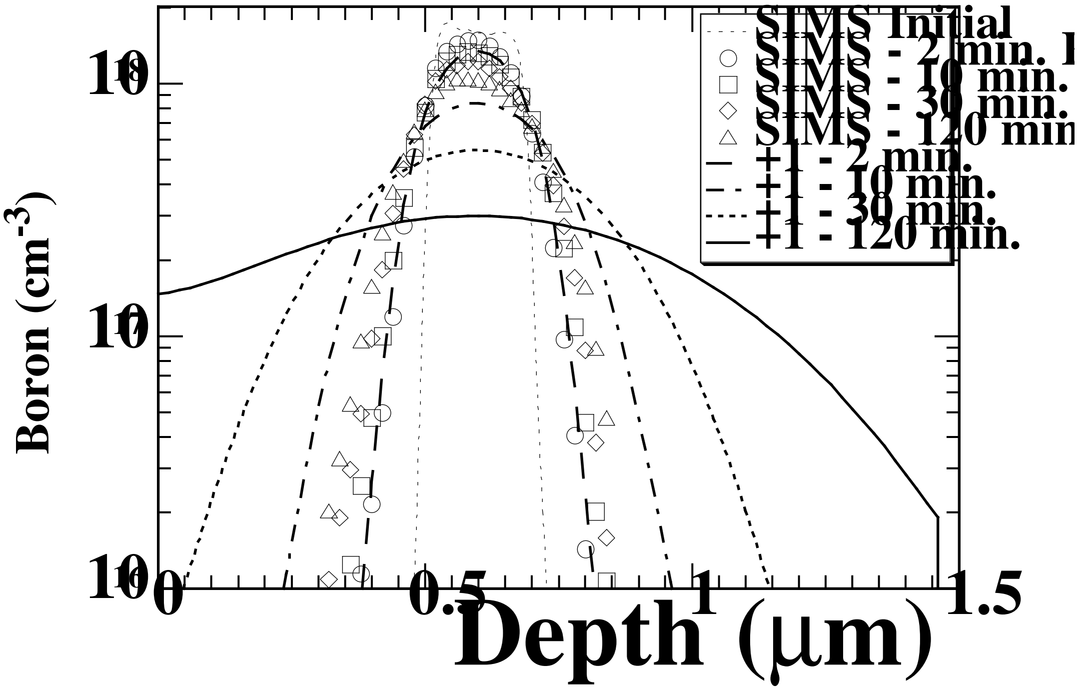

Figure 4.4 Comparison of simulation results using Packan s model and the full +1 approach compared to experimental data for a $4x10^{15}$ cm^{-2}, 50 keV silicon implanted sample annealed at 750ßC for 2, 10, 30, and 120 minutes. C_I^{max}/C_I^* was set to 15,025 in this simulation. The remaining simulation parameters are from [23] and are listed in Table 2.2 on page 27.

Packan proposed two possible mechanisms for the saturation effect in enhanced diffusion. The first explanation involves the dilute approximation which is used to derive the two.dim model equations, Eq. 4.4, Eq. 4.5, and Eq. 4.8. In the dilute approximation, the concentration of the mobile species, C_{AX}, is assumed to be much smaller than either the total dopant concentration or the total defect concentration. Under large point defect supersaturations such as after implantation, C_{AX} may not be dilute. In fact, when all of the dopant becomes paired with defects as mobile species, the maximum enhancement in dopant diffusivity will be attained. A nondilute equilibrium pair diffusion model has been implemented as the new full.cpl model in SUPREM-IV and will be described in detail in the next section. In the second explanation, implantation damage is proposed to generate interstitial clusters. Similar to the dislocation loops modeled in Chapter 2, due to the internal energy and strain energy of the cluster, C_I must be maintained at a new equilibrium concentration, $C^*_{I,cluster}$, which is greater than C_I^*, in order to sustain the clusters. Packan proposes that a stable distribution of interstitial clusters forms very quickly during the anneal. For short times, the interstitial concentration is maintained at $C^*_{I,cluster}$ without any significant change in the cluster size. Such a scenario would limit the interstitial supersaturation, and the maximum enhancement in dopant diffusivity, to $C^*_{I,cluster}/C^*_I$ until the clusters shrink appreciably.

In the nondilute equilibrium pairing approach, the maximum enhancement in dopant diffusivity for a predominantly interstitial diffuser is given by $1/K_{AI}C_I^*$ where K_{AI} is the equilibrium pairing constant between the dopant A and interstitials [72]. This value should be time-invariant at any given temperature since both K_{AI} and C_I^* are temperature activated parameters. Meanwhile, in the clustering approach, as the clusters shrink in size, $C^*_{I,cluster}$ will increase in a similar manner as $C^*_{I,loop}$ (see Eq. 2.12 from Chapter 2), namely, exponentially with the inverse radius of the clusters. Thus one would expect C_I^{max} to actually increase as a function of time as the clusters dissolve and shrink in size. So neither the nondilute equilibrium pair model nor the clustering model predicts that C_I^{max} decreases as a function of time bringing into question the exact physical process that manifests itself through C_I^{max}.

To this juncture, only the full +1 approach has been investigated. The exact same parameters were used as in Figure 4.4 except now the +1 profile was scaled down from a dose of 4x10^{15} cm^{-2} to a dose of 3x10^{12} cm^{-2}. In doing so, an additional fitting parameter has been introduced, and as shown in Figure 4.5, the scaled +1 approach fits the 2 and 30

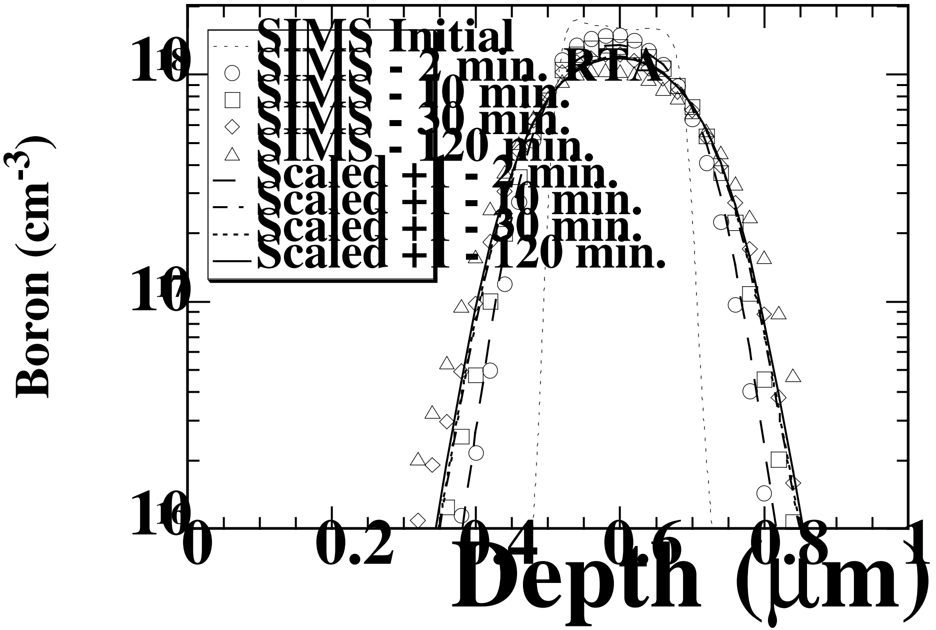

Figure 4.5 Comparison of simulation results using Packan s model and the scaled +1 approach compared to experimental data for a 4x10^{15} cm^{-2}, 50 keV silicon implanted sample annealed at 750ßC for 2, 10, 30, and 120 minutes. C_I^{max}/C_I^* was set to 15,025 in this simulation and the remaining simulation parameters are from [23] and are listed in Table 2.2 on page 27. The scaled +1 dose used was 3x10^{12} cm^{-2}.

minute time points at 750ßC but there is too much profile motion for the 10 minute anneal and not enough motion for the 120 minute anneal.

The main reason Packan s model does not match the time-dependence is because the model predicts only one time transition in the enhanced diffusion of the boron marker layer while the experimental data indicates two time transitions in the enhanced diffusion. This trend in the data is not obvious when looking at Figure 3.8 on page 63 from Chapter 3 because the time-averaged enhancements plotted in that figure are referenced with respect to the initial boron profile. Figure 4.6, on the other hand, plots the time-averaged

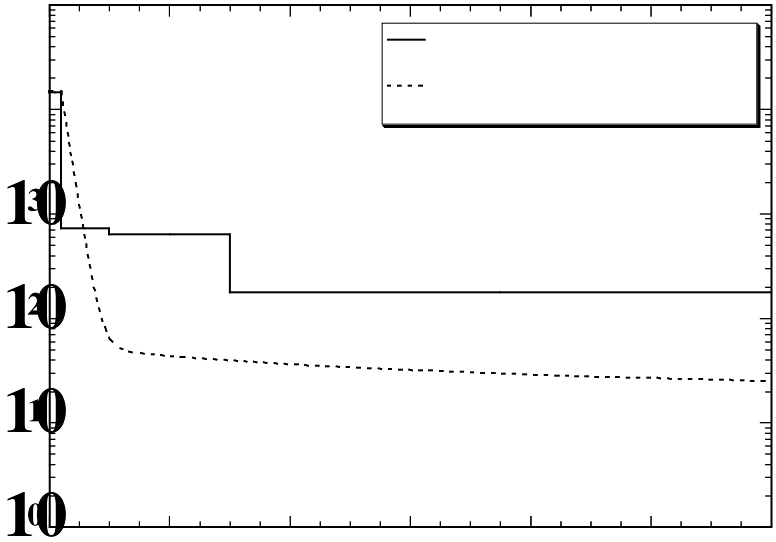

PostScript error

Figure 4.6 Comparison of the time-averaged enhancements in boron diffusivity between time points for the 4x10^{15} cm^{-2}, 50 keV silicon implanted samples annealed at 750ßC for 2, 10, 30, and 120 minutes to the simulated interstitial supersaturation at a depth of 0.6 µm using Packan s model and the scaled +1 approach.

enhanced diffusion between time points for the same data, i.e. the time-averaged enhancements from 0 to 2 minutes, from 2 to 10 minutes, from 10 to 30 minutes, and from 30 to 120 minutes. Figure 4.6 clearly shows that the enhanced diffusion exhibits at least two time transitions. The first transition occurs within 2 minutes at which point the enhanced diffusion remains relatively constant at a large value out to 30 minutes. A second transition occurs between 30 and 120 minutes. Also plotted in Figure 4.6 is the interstitial supersaturation, C_I/C^*_I, at a depth of 0.6 µm corresponding to the simulation result using Packan s model and the scaled +1 approach shown in Figure 4.5. If the simulation result agreed with the experimental data for all time points, then the interstitial supersaturation would track the time-averaged enhancements in diffusivity. However, as shown in the figure, the simulation result only predicts one time transition in the interstitial supersaturation.

Based on these full +1 and scaled +1 simulations, we conclude that Packan s model alone cannot accurately describe the time-dependent IED observed for our high-dose data presented in the previous chapter.

4.5.2 Park and Law Model

Park and Law have presented a nondilute equilibrium pair diffusion model which also predicts a saturation in implant-damage enhanced diffusion [72],[73]. Physically, for very large defect concentrations, the number of mobile species may no longer be dilute. In fact, the maximum enhancement in dopant diffusivity occurs when all of the dopant is paired with defects and is mobile. The motion of the dopant does not increase any more at this point even if additional point defects are created.

Park and Law were able to use this model in conjunction with defect traps to simulate Packan s data as well as their own data on low-dose IED of boron and phosphorus, respectively. The ability of their model to match high-dose data is investigated in this section.

The current diffusion models in SUPREM-IV all assume the dilute approximation in which the number of mobile dopant atoms is much less that the substitutional atoms. Thus, the nondilute equilibrium pair model of Park and Law was implemented into SUPREM-IV as the new full.cpl model. The following equations constitute the new full.cpl model:

$$\frac{\partial C_I^f}{\partial t} + \sum_A \frac{\partial C_{AI}}{\partial t} = \nabla\bullet\left(D_I \nabla C_I^f - \sum_A J_{AI}\right) - K_R\,(C_I^f C_V^f - C_I^* C_V^*) \qquad (4.13)$$

$$\frac{\partial C_V^f}{\partial t} + \sum_A \frac{\partial C_{AV}}{\partial t} = \nabla\bullet\left(D_V \nabla C_V^f - \sum_A J_{AV}\right) - K_R\,(C_I^f C_V^f - C_I^* C_V^*) \qquad (4.14)$$

$$\frac{\partial C_A^T}{\partial t} = \nabla\bullet\left[\left(D_{AI}\frac{C_I^f}{C_I^*}\frac{p}{n_i}\right)\nabla\, ln\left(C_A^S\frac{C_I^f}{C_I^*}\frac{p}{n_i}\right) + \left(D_{AV}\frac{C_V^f}{C_V^*}\frac{p}{n_i}\right)\nabla\, ln\left(C_A^S\frac{C_V^f}{C_V^*}\frac{p}{n_i}\right)\right] = -\nabla\bullet\,(J_{AI} + J_{AV}) \qquad (4.15)$$

$$C_{AI} = K_{AI} C_A^S C_I^f \qquad (4.16)$$

$$C_{AV} = K_{AV} C_A^S C_V^f \tag{4.17}$$

$$C_A^T = C_A^S + C_{AI} + C_{AV} \tag{4.18}$$

$$C_I^T = C_I^f + \sum_A C_{AI} \tag{4.19}$$

$$C_V^T = C_V^f + \sum_A C_{AV} \tag{4.20}$$

where the variables not previously defined are now defined as follows:

C_I^f: free interstitial concentration
C_{AI}: dopant/interstitial pair concentration
C_V^f: free vacancy concentration
C_{AV}: dopant/vacancy pair concentration
C_A^S: substitutional dopant concentration
C_A^T: total dopant concentration
K_{AI}: equilibrium dopant/interstitial pair constant
K_{AV}: equilibrium dopant/vacancy pair constant.

Currently only pairing with neutral defects has been implemented. In comparison to the old full.cpl model (Eq. 4.8, Eq. 4.11, and Eq. 4.12), the total defect and dopant concentrations have been replaced by the free and substitutional concentrations, respectively. The model is an equilibrium model because the paired species, C_{AI} and C_{AV}, are not new solution variables in SUPREM-IV. They are calculated from Eq. 4.16, Eq. 4.17, and Eq. 4.18 using the equilibrium pairing constants, K_{AI} and K_{AV}, and the concentrations already solved by SUPREM-IV, namely C_I^f, C_V^f, and C_A^T. The maximum enhancement that can be achieved using this model is $1/(K_{AI}C_I^*)$ or $1/(K_{AV}C_V^*)$ depending on whether the dopant diffuses primarily with interstitials or vacancies, respectively [72].

Using the same parameter set as Park and Law [72] and using the full +1 initial interstitial profile resulted in very poor fits to the data. Similar to the full +1 simulation using Packan s model, even if K_{BI}, the equilibrium boron/interstitial pairing constant, is changed to fit the 2 minute data point, too much diffusion occurs for the longer time points. This is due to the fact that the interstitial concentration remains high enough throughout the entire simulation that the maximum enhancement in boron diffusivity is maintained. An extensive matrix of simulations was performed varying several parameters including the scaled +1 concentration, D_I, K_{BI}, D_V, K_B, and K_s^I. In most cases the fits were very poor and in no case did the simulation result match the experimental data for all four anneal times. Figure 4.7 compares the time-averaged enhanced diffusion to the simulated interstitial supersaturation at a depth of 0.6 µm using Park and Law s model and the scaled +1 approach. It is quite evident from this figure that the reason why Park and

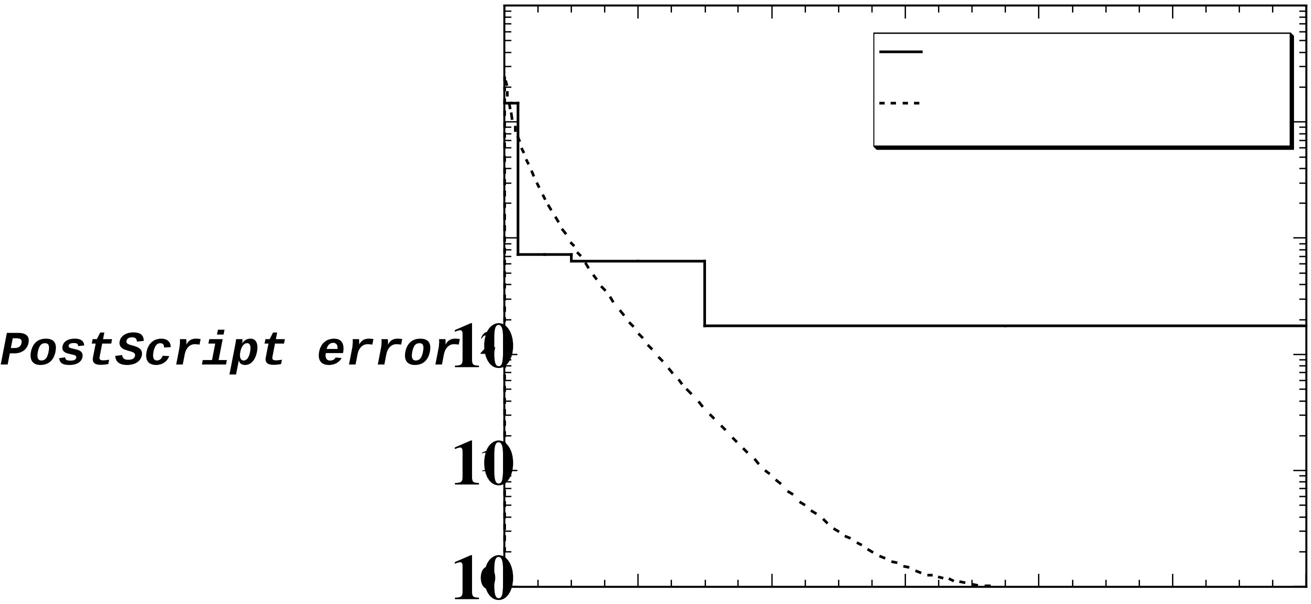

Figure 4.7 Comparison of the time-averaged enhancements in boron diffusivity between time points for the 4×10^{15} cm^{-2}, 50 keV silicon implanted samples annealed at 750ßC for 2, 10, 30, and 120 minutes to the simulated interstitial supersaturation at a depth of 0.6 µm using Park and Law s model and the scaled +1 approach. Parameters from Park and Law [72] were used in this simulation except K_{BI}, the equilibrium boron/interstitial pairing constant, was decreased to 6×10^{-18} cm^3. A scaled +1 dose of 1.1×10^{12} cm^{-2} was used as the initial interstitial profile.

Law s model cannot fit all four time points is because this model also predicts only one time transition in the enhanced diffusion.

Since the 2 minute data point is actually a 745ßC, 2 minute RTA anneal, a large matrix of simulations was done to try and optimize the simulated results to only the 10, 30, and 120 minute data points. In this case, the scaled +1 approach was used, and only D_I, K_{BI}, and D_V were varied. K_B, the $D_IC_I^*$ and $D_VC_V^*$ products, and the D_I/K_S^I quotient were taken from Table 4.2. A parameter set was obtained which matched just the three longer data points (see Figure 4.8). However, the model and parameters should also match data

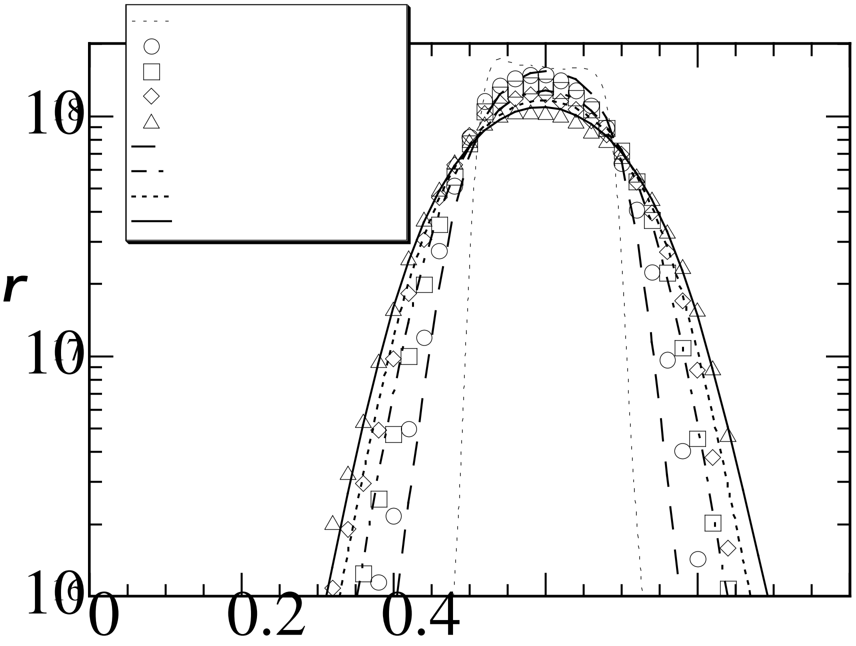

Figure 4.8 Comparison of simulation results for the $4x10^{15}$ cm^{-2}, 50 keV silicon implanted samples annealed at 750ßC for 2, 10, 30, and 120 minutes using Park and Law s model and an initial interstitial profile of $6x10^{12}$ cm^{-2}. D_I=2.15x10^{-11} cm^2/s, D_V=1x10^{-11} cm^2/s, and K_{BI}=2.15x10^{-20} cm^3. K_B, $D_IC_I^*$, $D_VC_V^*$, and D_I/K_S^I are taken from Table 4.2.

for other implant conditions. In particular, our experimental data combined with Packan s data [11] and Crowder s data [74] indicates that low-dose implants exhibit an initially large enhancement in diffusivity that decays very quickly with time while moderate and high-dose implants exhibit two time transitions in enhanced diffusion, one initially large enhancement that decays very quickly followed by a longer time enhancement which is lower in magnitude than the initial enhancement but still substantial enough that significant dopant diffusion occurs.

The same parameters used to generate the simulation results in Figure 4.8 were used to try and simulate recent low-dose results of Crowder [74]. In Crowder s experiment, a 2x10^{13} cm^{-2}, 35 keV silicon implant was annealed at 750ßC for times between 30 seconds and 45 minutes. Most of the enhanced diffusion of a buried boron marker layer occurred within the first 30 seconds. In order to get a reasonable match to the 30 second SIMS data, a 3x10^{13} cm^{-2} scaled +1 profile had to be used (see Figure 4.9). Note the asymmetry in the 30 second simulated profile. Even more important, though, is that the simulation result predicts too much profile broadening for longer times. The 2 minute simulation in Figure 4.9 has continued to broaden significantly while the 30 minute SIMS data has hardly

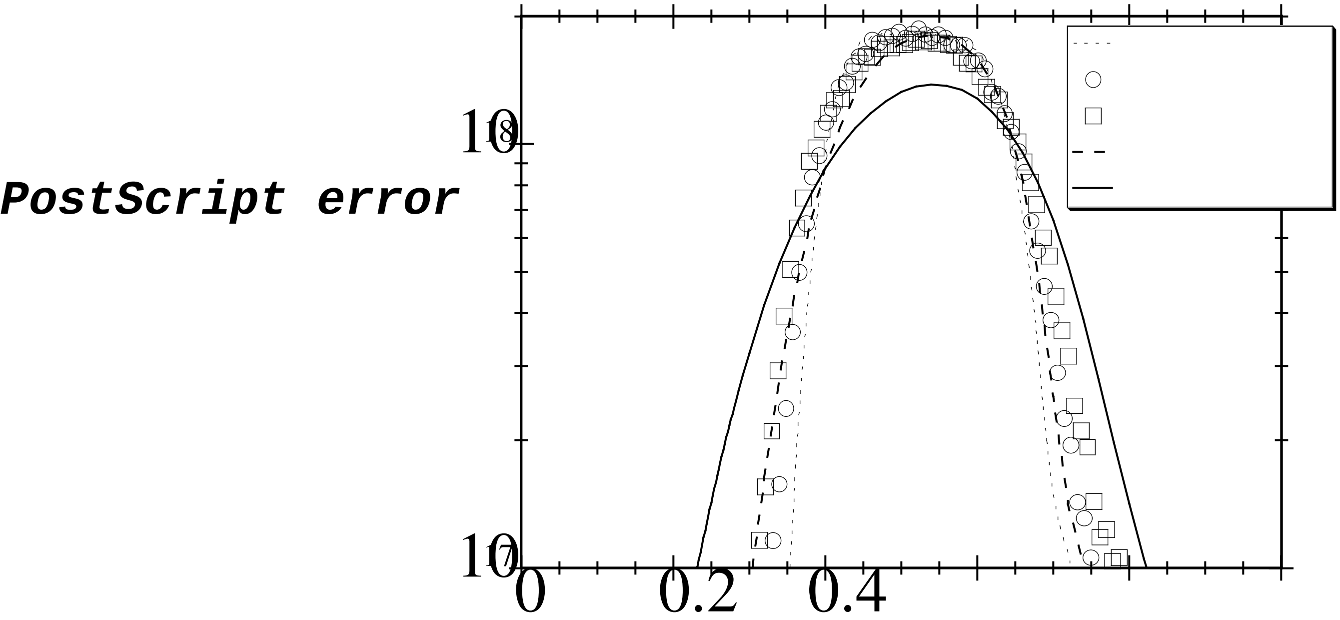

Figure 4.9 Comparison of simulation results for 2x10^{13} cm^{-2}, 35 keV silicon implanted samples annealed at 750ßC using the same parameter set as in Figure 4.8 except a scaled +1 dose of 3x10^{13} cm^{-2} was used. SIMS data from Crowder [74].

moved compared to the 30 second data. Thus although a parameter set can be obtained which is sufficient for a particular data set, the model and parameter set is not applicable to a broad range of experimental conditions.

If the scaled +1 approach is used rather than the full +1 method, then only short time points can be fit. In these cases, we were able to fit the short-time data, but not the long-time data using extremely small values of K_{BI} such that the full.cpl model reduces to the two.dim model. Figure 4.10 shows simulation results using the two.dim model, a 3.5×10^{12} cm^{-2} scaled +1 interstitial profile, and the parameters listed in Table 4.2. Note the good fit at short anneal times, but not long anneal times. Additional motion is observed in the long-time data whereas the enhanced diffusion in the simulation stops after just 10 minutes. Figure 4.11 shows simulation results compared to SIMS data for the samples that received the same 4×10^{15} cm^{-2}, 50 keV silicon implants, but were annealed at 800ßC. The same

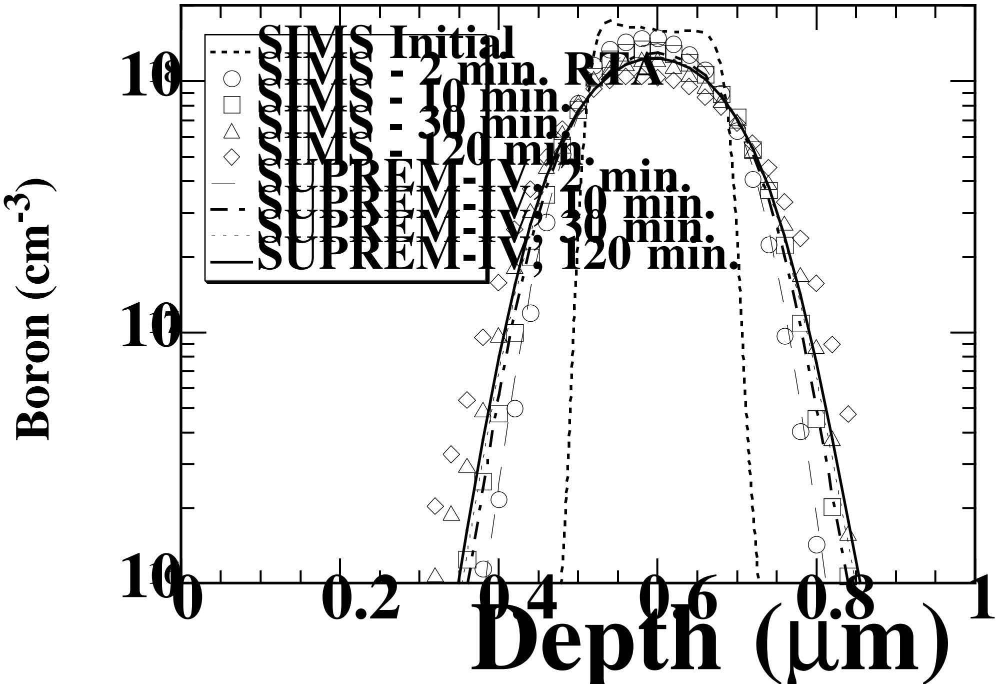

Figure 4.10 Comparison of simulation results for the 4×10^{15} cm^{-2}, 50 keV silicon implanted samples annealed at 750ßC for 2, 10, 30, and 120 minutes using the two.dim model and an initial interstitial profile of 3.5×10^{12} cm^{-2}.

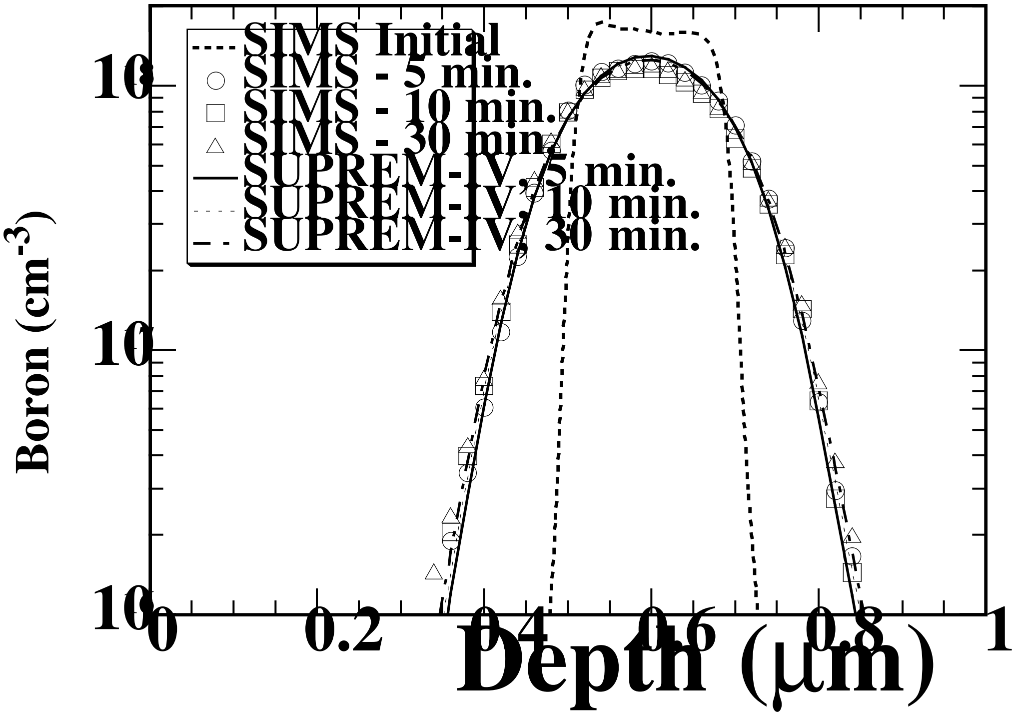

Figure 4.11 Comparison of simulation results for the 4x10^{15} cm^{-2}, 50 keV silicon implanted samples annealed at 800ßC for 5, 10, and 30 minutes using the two.dim model and an initial interstitial profile of 3.5x10^{12} cm^{-2}.

Parameter	Value	Reference
D_I	1.03x10^{6} exp(-3.22/kT) cm^{2}/s	Boit *et al.* [75]
C_I^*	3.1x10^{19} exp(-1.58/kT) cm^{-3}	Boit *et al.* [75]
K_S^I	74.6 exp(-1.53/kT) cm/s	Crowder *et al.* [76]
D_V	6.34x10^{3} exp(-3.29/kT) cm^{2}/s	Law [79]
C_V^*	4.77x10^{18} exp(-0.713/kT) cm^{-3}	Law [79]
K_S^V	1.11x10^{3} exp(-2.63/kT) cm/s	Griffin [78]
K_B	1.40 exp(-3.99/kT) cm^{3}/s	Law [79]

Table 4.2 Parameter set used to simulate short-time IED. D_I is the interstitial diffusivity, C_I^* is the equilibrium interstitial concentration, K_S^I is the inert interstitial surface recombination velocity, D_V is the vacancy diffusivity, C_V^* is the equilibrium vacancy concentration, K_S^V is the inert vacancy surface recombination velocity, K_B is the bulk recombination coefficient.

scaled +1 interstitial profile of 3.5x10^{12} cm^{-2} that was used to fit the short-time data at 750ßC was used here, and again, good fits are obtained for short times, but additional profile broadening occurs for longer anneal times that is not predicted by the simulations.

The two.dim model and the scaled +1 approach along with the parameter set in Table 4.2 not only matches our high-dose, short-time data, but is also consistent with low-dose data. Figure 4.12 compares simulations using the parameters in Table 4.2 and a scaled +1 dose of 2x10^{12} cm^{-2} to Crowder s 2x10^{13} cm^{-2}, 35 keV silicon implanted samples annealed at 750ßC. This time the simulation results for both the 30 second and 30 minute anneals agree much better with the SIMS data. Recall that in Figure 4.9, when the new full.cpl model was used, the time dependence of Crowder s low-dose data could not be simulated using a parameter set previously extracted for the high-dose data. Also, note that the scaled +1 dose used for this low-dose case (2x10^{12} cm^{-2}) is very similar in magnitude to the scaled +1 dose used for the high-dose experiment (3.5x10^{12} cm^{-2}).

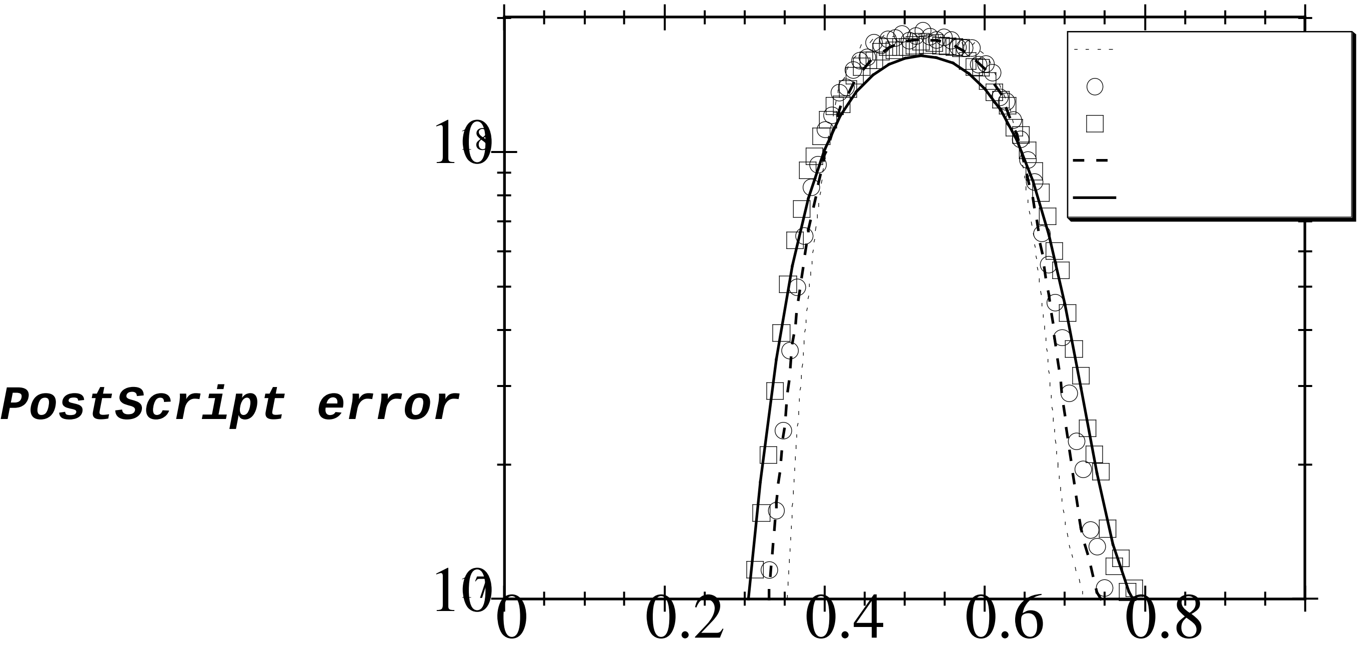

Figure 4.12 Comparison of simulation results for 2x10^{13} cm^{-2}, 35 keV silicon implanted samples annealed at 750ßC using a scaled +1 dose of 2x10^{12} cm^{-2} and the parameters from Table 4.2. SIMS data from Crowder [74].

To conclude this section, a nondilute equilibrium pair diffusion model was implemented into SUPREM-IV as the new full.cpl model. Unfortunately, a single parameter set that applies to both low and high-dose implantation damage could not be obtained because of the different time dependences in enhanced diffusion for the two cases. However, for short anneal times, the simpler two.dim model is sufficient for modeling both high-dose and low-dose data. The new full.cpl model may be important for cases in which the dopant itself is used to create the damage. Meanwhile, the standard full.cpl model remains important for simulating high-concentration phosphorus diffusion in order to obtain the characteristic kink-and-tail profiles.

4.6 Modeling the Two Time Transitions of IED

4.6.1 Short-time Transition

Figure 4.10 and Figure 4.11 show two.dim simulation results using the parameters from Table 4.2 for the 4x10^{15} cm^{-2}, 50 keV silicon implanted samples annealed at 750ßC and 800ßC, respectively for various anneal times. Good fits are obtained for short times in both figures. The initial interstitial profile was scaled to 3.5x10^{12} cm^{-2} in these simulations. Figure 4.13, Figure 4.14, and Figure 4.15 show two.dim simulation results for the 1x10^{14} cm^{-2}, 80 keV silicon implanted samples annealed at 750ßC, 800ßC, and 850ßC, respectively using the same parameter set given in Table 4.2. A 5x10^{12} cm^{-2} scaled +1 profile was used as the initial interstitial concentration for these simulations. Finally, Figure 4.16 and Figure 4.17 show two.dim simulation results for the 2x10^{15} cm^{-2}, 100 keV silicon implanted samples annealed at 750ßC and 800ßC, respectively, also using the parameter set from Table 4.2. In this case, a 4x10^{12} cm^{-2} scaled +1 profile was used as the initial interstitial concentration. Although the same scaled +1 profile was not used for each implant condition, the actual doses used are all of the same order of magnitude and are much less than the total implanted dose. This is reasonable given that we have shown in Chapter 3 that the enhanced diffusion for moderate (1x10^{14} cm^{-2}) to high-dose implants (1x10^{16} cm^{-2}) for short anneal times is independent of dose. The fact that the necessary

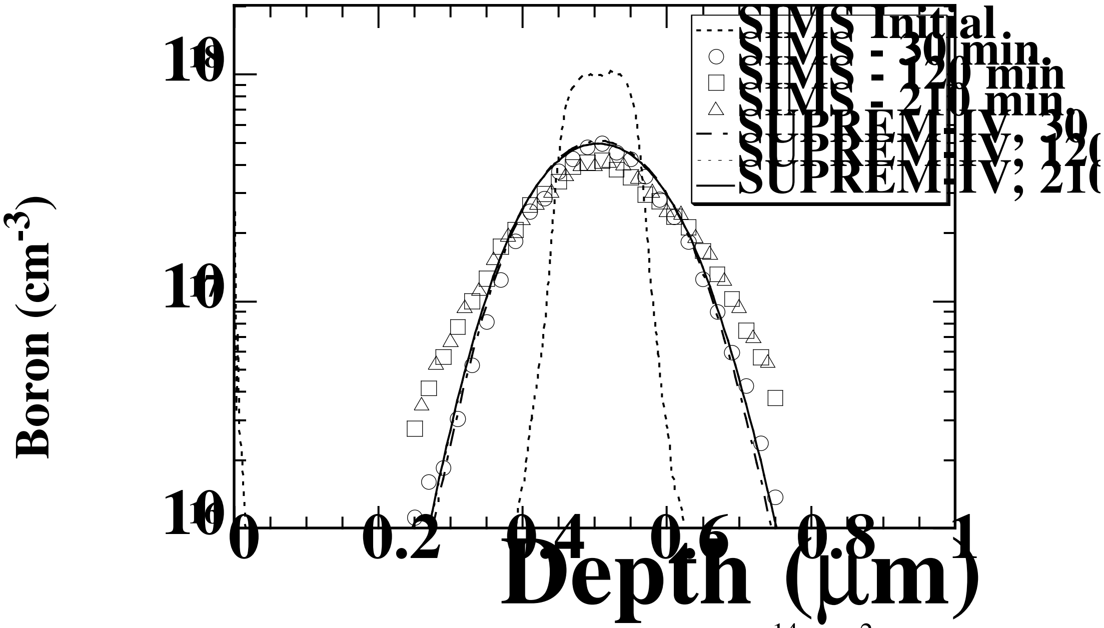

Figure 4.13 Comparison of simulation results for the 1x10^{14} cm^{-2}, 80 keV silicon implanted samples annealed at 750ßC for 30, 120, and 210 minutes using the two.dim model and an initial interstitial profile of 5x10^{12} cm^{-2}.

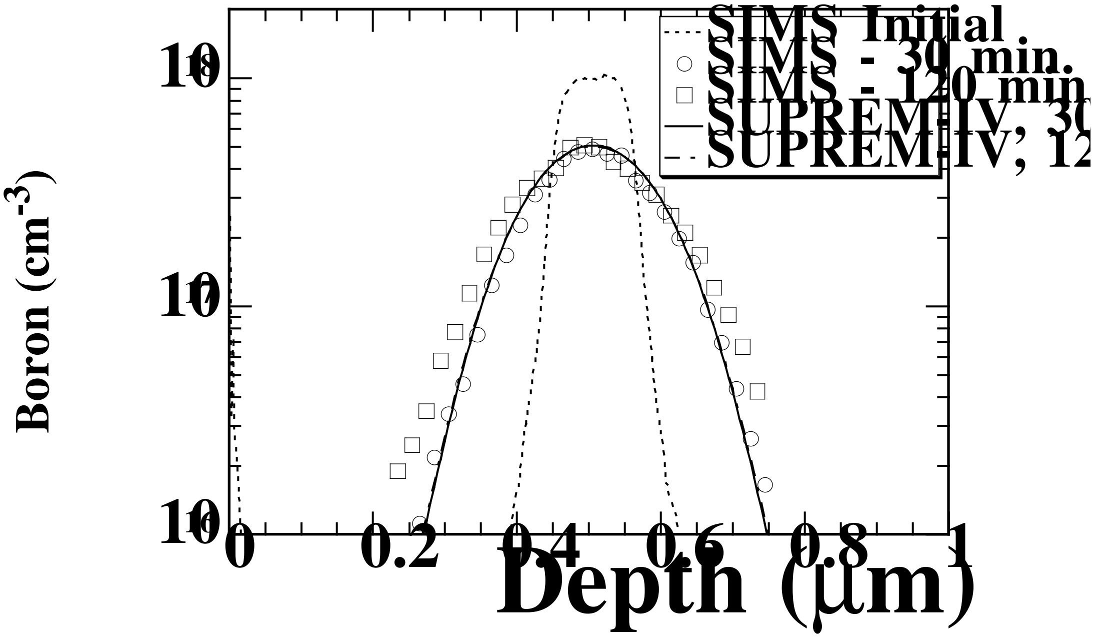

Figure 4.14 Comparison of simulation results for the 1x10^{14} cm^{-2}, 80 keV silicon implanted samples annealed at 800ßC for 30 and 120 minutes using the two.dim model and an initial interstitial profile of 5x10^{12} cm^{-2}.

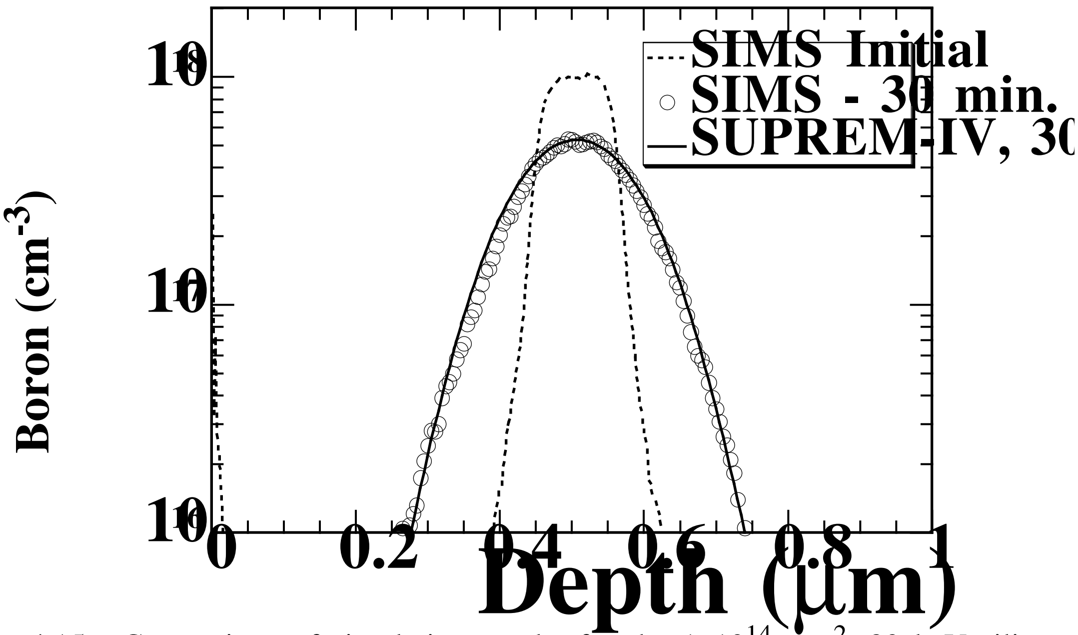

Figure 4.15 Comparison of simulation results for the 1x10^{14} cm^{-2}, 80 keV silicon implanted samples annealed at 850ßC for 30 minutes using the two.dim model and an initial interstitial profile of 5x10^{12} cm^{-2}.

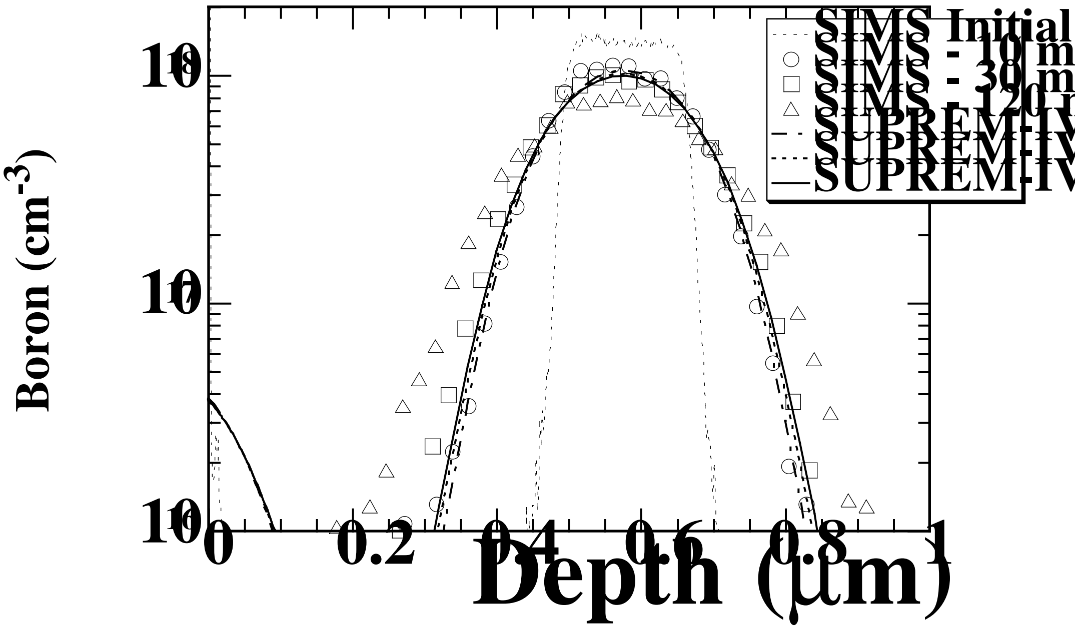

Figure 4.16 Comparison of simulation results for the 2x10^{15} cm^{-2}, 100 keV silicon implanted samples annealed at 750ßC for 10, 30, and 120 minutes using the two.dim model and an initial interstitial profile of 4x10^{12} cm^{-2}.

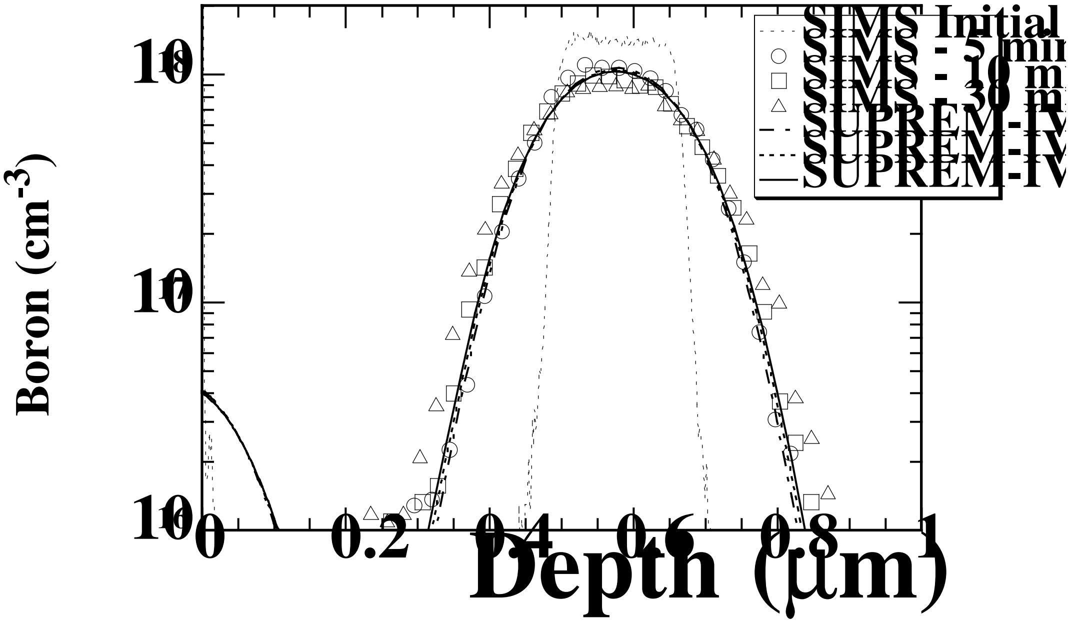

Figure 4.17 Comparison of simulation results for the $2x10^{15}$ cm^{-2}, 100 keV silicon implanted samples annealed at 800ßC for 5, 10, and 30 minutes using the two.dim model and an initial interstitial profile of $4x10^{12}$ cm^{-2}.

scaled +1 profiles are not identical for the different implant conditions can be attributed to the energy dependence observed in Section 3.2.1.2 where higher implant energies resulted in larger enhancements in boron diffusivity. However, for a given implant dose and energy, the same scaled +1 profile can be used to fit short-time data at more than one temperature providing additional support for the scaled +1 model.

Furthermore, only one parameter set (see Table 4.2) was used in all of these simulations. This parameter set was shown in Section 4.5.2 to accurately model the time-dependent enhanced diffusion for a low-dose silicon implant and has also been used by Crowder *et al.* [76] to simulate low-dose boron IED in silicon-on-insulator material in the temperature range from 600ßC to 900ßC. That a single parameter set is applicable to both low and high-dose IED for short anneal times is another indication that we have taken the correct modeling approach.

These results strongly indicate that for moderate to high-dose implants, there are two time transitions related to IED. The first short-time transition can be attributed to the initial point defect concentrations returning to their equilibrium values via diffusion and recombination. The source of the second long-time transition is discussed in the next section.

4.6.2 Long-time Transition

Others have proposed that more than one physical mechanism is responsible for IED. Schreutelkamp *et al.* [80] observed that the enhanced tail diffusion of implanted boron is similar for low-dose ($1x10^{13}$ cm^{-2}) and high-dose ($5x10^{15}$ cm^{-2}) implants annealed for very short times (10 - 20 seconds) at high temperatures (900ßC and above). Additional enhanced diffusion was observed only for the high-dose implants for longer annealing times (minutes) at 1000ßC. This additional enhanced diffusion was attributed to the dissolution of interstitial-type extended defects and was qualitatively verified via channeling RBS and some TEM measurements.

Schreutelkamp proposed two annealing stages for implant doses above the threshold for extended defect formation. In the first stage, enhanced tail diffusion occurs due to the excess interstitial concentration generated by the implant itself. At the same time, some of the point defects agglomerate to form extended defects. During the second stage, for long anneal times, the extended defects anneal partially or completely resulting in additional enhanced diffusion.

Kim *et al.* [81] observed similar results for a $1x10^{15}$ cm^{-2}, 40 keV phosphorus implant. Enhanced tail diffusion saturated within 15 seconds during a 900ßC RTA anneal. RTA anneals for an additional 15 seconds and 45 seconds did not change the phosphorus profile. However, an additional 850ßC, 1 hour furnace anneal resulted in further profile broadening (see Figure 4.18). Kim attributed this behavior to two sources for interstitial defects. The first source, responsible for the short-time enhanced diffusion during the RTA, was due to the dissolution of interstitial-type point defect clusters. The second source, responsible for the enhanced diffusion during the subsequent furnace anneal, was due to the annealing of end-of-range interstitial dislocation loops.

Cowern [82] has also pointed out that the transient enhanced diffusion after implantation lasts longer for higher dose implants. Cowern used molecular beam epitaxy

Figure 4.18 Enhanced diffusion after a 1x10^{15} cm^{-2}, 40 keV phosphorus implant. The enhanced diffusion saturates within 15 seconds during the 900ßC RTA. However, additional motion occurs for a subsequent, 850ßC, 1 hour furnace anneal (Reproduced from Kim *et al.* [81]).

(MBE) to grow double boron marker layers. The samples were implanted with silicon at doses of either 1x10^{13} cm^{-2} or 1x10^{14} cm^{-2} then RTA annealed at 800ßC for 10 seconds to 30 minutes. For the 1x10^{13} cm^{-2} implanted samples, the enhanced diffusion was over after only 10 seconds while enhanced diffusion continued for the 1x10^{14} cm^{-2} implanted samples for 15 minutes. Cowern attributed the short-time enhancement that occurred for both doses to the generation of interstitial boron atoms kicked out by the tails of the silicon implants. These interstitial boron atoms travel long distances before returning to substitutional sites [55]. Cowern attributed the longer time enhancement present for the higher dose implant to the dissolution of interstitial-type clusters which were measured via TEM analysis. Clusters were found in the 1x10^{14} cm^{-2} implanted sample annealed at 10 seconds, but not in the sample annealed for 100 seconds.

Finally, Angelucci *et al.* [83] have shown that enhanced phosphorus diffusion during 750ßC furnace annealing lasts as long as a positive strain remains in the surface region of the implanted sample. The strain measurements were performed using double crystal x-ray diffraction (DCD) [84]. The authors claim that the positive strain indicates the presence of interstitial-type clusters. Cembali *et al.* [85] have compared DCD measurements with a TEM measurement of a sample implanted with 1x10^{14} cm^{-2} silicon at 60 keV and found that point defect clusters approximately 25 in radius were observed in the TEM measurement at depths corresponding to the region in which a positive strain was measured using the DCD technique.

In all of the above studies, the dissolution of extended defects or point defect clusters was proposed to account for the enhanced dopant diffusion after ion implantation for long anneal times. Recall that the data presented in Chapter 3 (which we are attempting to model) spans implant doses both below and above the amorphization threshold. Implant doses below the amorphization threshold do not always generate extended defects. However, the lowest implant dose in this study (1x10^{14} cm^{-2}, 80 keV) is similar to Cowern s 1x10^{14} cm^{-2}, 50 keV implant condition where the presence of interstitial clusters was verified via TEM analysis [82]. Thus we assume that the dissolution of interstitial clusters is responsible for the long-time enhancements observed by us and others.

4.6.3 Using Dislocation Loop Model to Mimic Cluster Dissolution

Although the exact structure of the interstitial clusters is not known, we assume they are disc-shaped so that our model for dislocation loops from Chapter 2 can be applied to interstitial clusters. Our model for dislocation loops contains the essential elements for a cluster model. First, the equilibrium interstitial concentration surrounding the cluster depends on both the cluster energy and the strain energy. This dependence is included in Eq. 2.12 of Chapter 2. Second, the interstitials absorbed or released by the clusters must be accounted for in the interstitial continuity equation as in Eq. 2.13. When C_I is less than $C^*_{I,loop}$ then the defect will dissolve releasing free interstitials which contribute to the enhanced diffusion of the boron marker layer.

Simulations using the dislocation loop model can, with one modification, lead to a long-time transition in enhanced diffusion. The scaled +1 approach is combined with the dislocation loop model to show the feasibility of a two-time transition modeling approach. Agreement between simulations and our experimental data out to 120 minutes at 750ßC is shown for several implant energies.

4.6.3.1 Time-Dependence of Loop Dissolution

In this section, the model for dislocation loop growth is evaluated, without any modification, to see whether or not it can generate the long-time enhanced diffusion that has been observed experimentally. As pointed out in Section 4.5.1, for the $4x10^{15}$ cm^{-2}, 50 keV implanted samples annealed at 750ßC, the long-time transient should begin around 30 minutes and last until 120 minutes.

Figure 4.19 shows the evolution of the interstitial concentration for a single plane of loops centered at 0.175 µm with an initial radius of 11 and a density of $4.5x10^{9}$ cm^{-2}. In reality, the clusters would be distributed over a larger volume. Simulations using multiple planes but keeping the total number of loops constant by decreasing the density have also been done. However, the simulated enhancements in the boron diffusivity are identical whether one or several planes of loops is used. As long as the total number of loops is kept constant, the enhancements are the same. For this reason, only one plane of loops is used in all subsequent simulations. The parameters from Table 4.2 were used and K_{loop} of 0.5 was used in the simulation. The interstitial supersaturation required to sustain loops varies exponentially with 1/r where r is the radius of the loop. This dependence makes the loops dissolve very quickly for small-sized loops as shown in Figure 4.19 in which the loops have completely dissolved in less than 1 second. In all of these simulations, once the loops shrink to less than 10 in size, they are ignored. At this point, the dissolved loops have generated an excess interstitial profile still centered around 0.175 µm. This profile will diffuse and recombine until C_I reaches equilibrium. The time-dependence for this process is identical to the time-dependence of the decay of the scaled +1 profile. This was shown in Section 4.5.2 to last only 10 minutes at 750ßC. Thus, the time-dependence for small clusters does not last long enough to match the long-time enhanced diffusion.

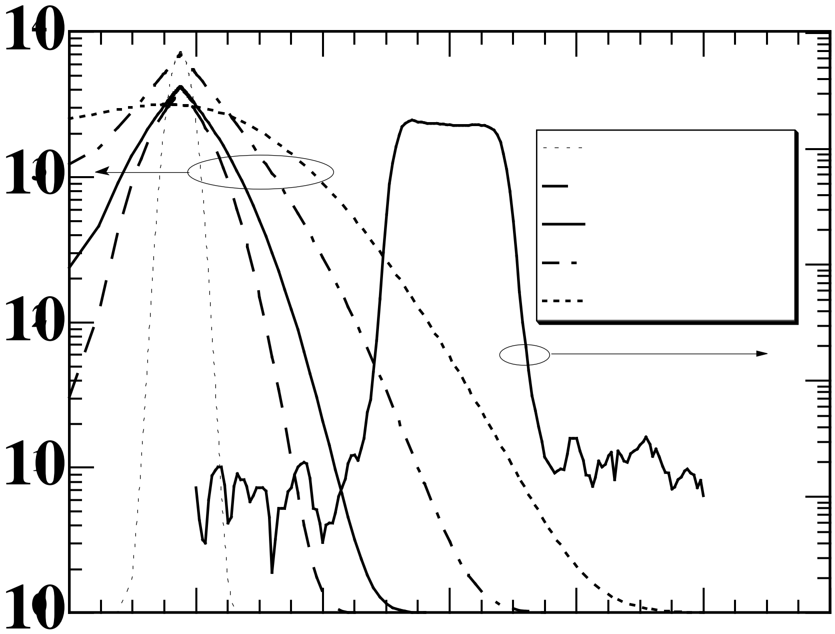

PostScript error

Figure 4.19 Interstitial evolution using the dislocation loop model to mimic cluster dissolution. The clusters become less than 10 in radius in less than 1 second. The clusters were centered at 0.175 μm from the surface with an initial radius of 11 and a density of 4.5x10^{9} cm^{-2}. K_{loop} was set to 0.5 in this simulation.

In order to make the time dependence longer, loops with a larger initial radius are used. Figure 4.20 shows the interstitial evolution for loops with an initial radius of 25 . In this case, it takes about 15 minutes for the loops to dissolve. We have increased the length of the transient due to loop dissolution. However, because of the exponential dependence of $C^{*}_{I,loop}$ on 1/r, the interstitial supersaturation actually increases during the anneal. This results in enhanced boron diffusion that also increases as a function of time. Unfortunately, our data does not support such a trend, and we are not aware of any data that corroborates this prediction. Thus, we conclude that without any modifications, the loop model is not able to quantitatively match the two time transitions in the enhanced diffusion for the 4x10^{15} cm^{-2}, 50 keV silicon implanted samples annealed at 750ßC.

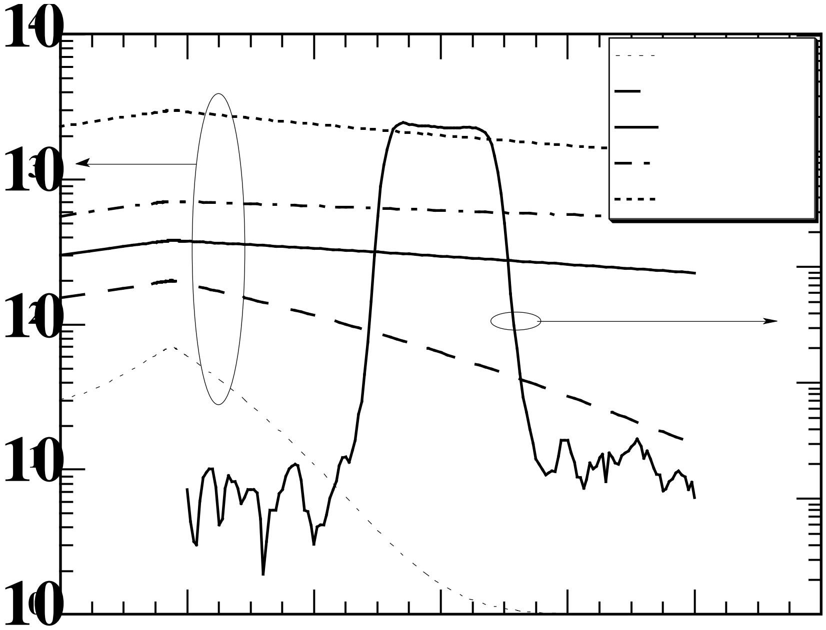

PostScript error Figure 4.20 Interstitial evolution using the dislocation loop model to mimic cluster dissolution. The initial radius in this case was 25 . All other parameters were identical to Figure 4.19.

4.6.3.2 Limiting Dissolution Rate

In order to extend the time over which the loops dissolve, the dissolution rate cannot be allowed to increase exponentially. The dissolution rate is limited to a constant for very small radii by placing a maximum value on $C^*_{I,loop}/C_I^*$. Possible physical reasons why the dissolution rate does not increase infinitely with 1/r are given in the next section.

Figure 4.21, Figure 4.22, and Figure 4.23 show simulation results for three different silicon implant damage conditions using loops centered at 0.175 µm with an initial radius of 10 , a density of $1.35\mathrm{x}10^{10}$ cm^{-2}, and K_{loop} equal to 0.35. In Figure 4.21, a $5\mathrm{x}10^{12}$ cm^{-2} scaled +1 profile was used as the starting interstitial profile. In Figure 4.22, an $8\mathrm{x}10^{12}$ cm^{-2} scaled +1 was used, and in Figure 4.23, a $7\mathrm{x}10^{12}$ cm^{-2} scaled +1 was used. The different scaled +1 values used for the three implants are representative of the energy dependence of enhanced diffusion in which larger enhancements are observed for higher energy damage implants. $C^*_{I,loop}/C_I^*$ was limited to 1500 in these simulations. The

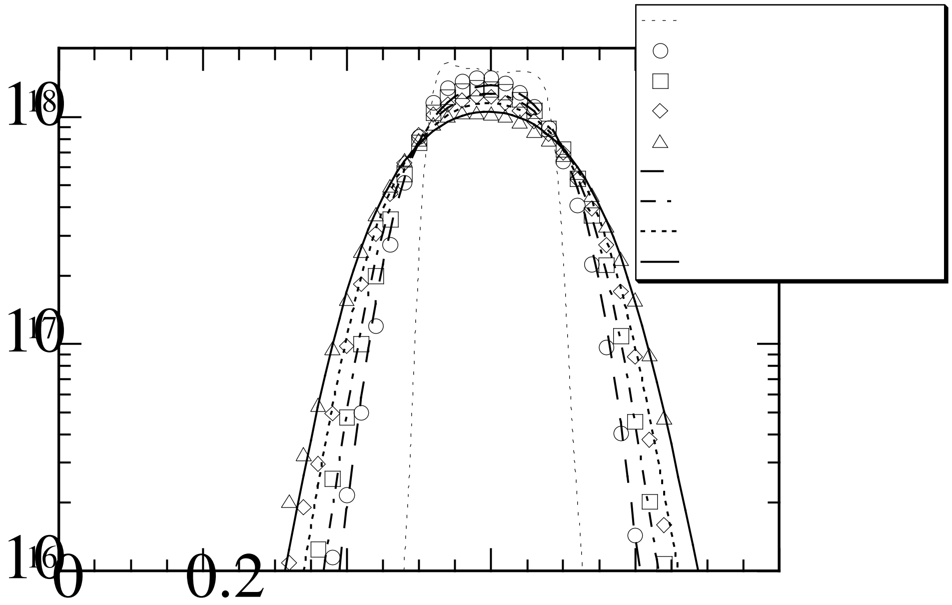

PostScript

Figure 4.21 Simulation fits to the $4x10^{15}$ cm^{-2}, 50 keV implanted samples annealed at 750ßC using the scaled +1 approach and the model for dislocation loops. A $5x10^{12}$ cm^{-2} scaled +1 profile was used. The loops were centered at 0.175 µm, the initial radius of the loops was 10 , the density of the loops was $1.35x10^{10}$ cm^{-2}, and K_{loop} was 0.35.

simulations show good fits to all time points out to 120 minutes. Note that the loops grow initially due to the excess interstitial concentration from the scaled +1 profiles. Eventually, the interstitial concentration decreases and the loops begin dissolving. Figure 4.24 compares the interstitial supersaturation to the time-averaged enhanced diffusion for the $4x10^{15}$ cm^{-2}, 750ßC annealed samples. By adding the dissolution of dislocation loops to the scaled +1 profile, two time transitions can now be obtained, the first one due to the decay of the scaled +1 profile, and the second one due to the dissolution of the dislocation loops.

4.6.3.3 Possible Physical Explanations for Limitation of the Dissolution Rate

Hu s original theory for stacking fault growth, which the dislocation loop model is based on, assumes that the particles lie in an infinite crystal and are noninteracting.

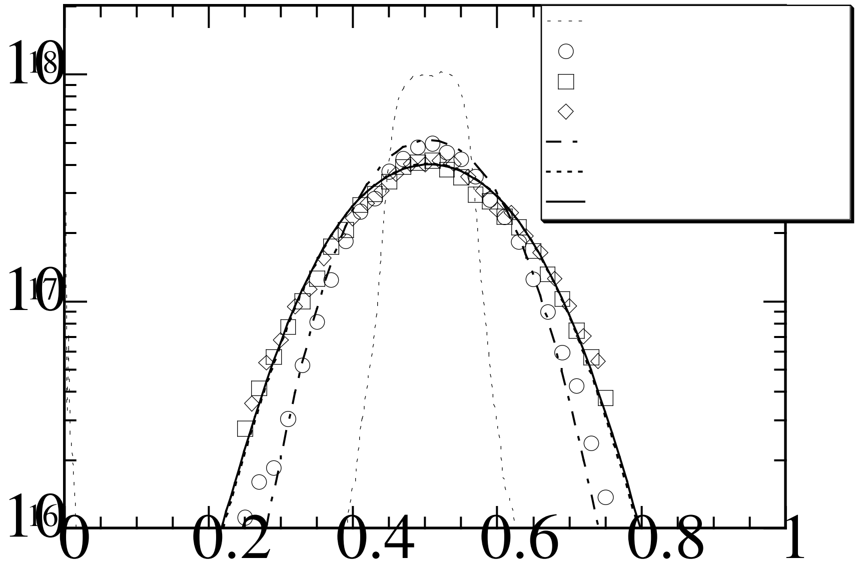

PostScript

Figure 4.22 Simulation fits to the 1x10^{14} cm^{-2}, 80 keV implanted samples annealed at 750ßC using the scaled +1 approach and the model for dislocation loops. An 8x10^{12} cm^{-2} scaled +1 profile was used. The loops were centered at 0.175 µm, the initial radius of the loops was 10 , the density of the loops was 1.35x10^{10} cm^{-2}, and K_{loop} was 0.35.

Obviously, these assumptions may not be true for the interstitial clusters which have been proposed to account for the long-time transient in enhanced boron diffusion. If the clusters are strongly interacting then the equilibrium interstitial concentration can be lower than predicted by Eq. 2.12 due to relaxation of the clusters [87]. In addition, the surface may play a role in limiting the maximum amount of strain which the clusters could attain. This would limit the equilibrium interstitial concentration surrounding the clusters.

Impurities and/or dopants may also be decorating the kink sites of the clusters thereby reducing the number of available sites for reaction and slowing down the dissolution rate [87]. Since there is very little dopant in the surface region of these samples, impurities are the more likely candidate.

Finally, if the clusters lie within a dislocation array that contains extended defects, the interstitial equilibrium concentration may actually be limited by the kinetics of the array rather than the individual point defect clusters. In this scenario, the growth or shrinkage of

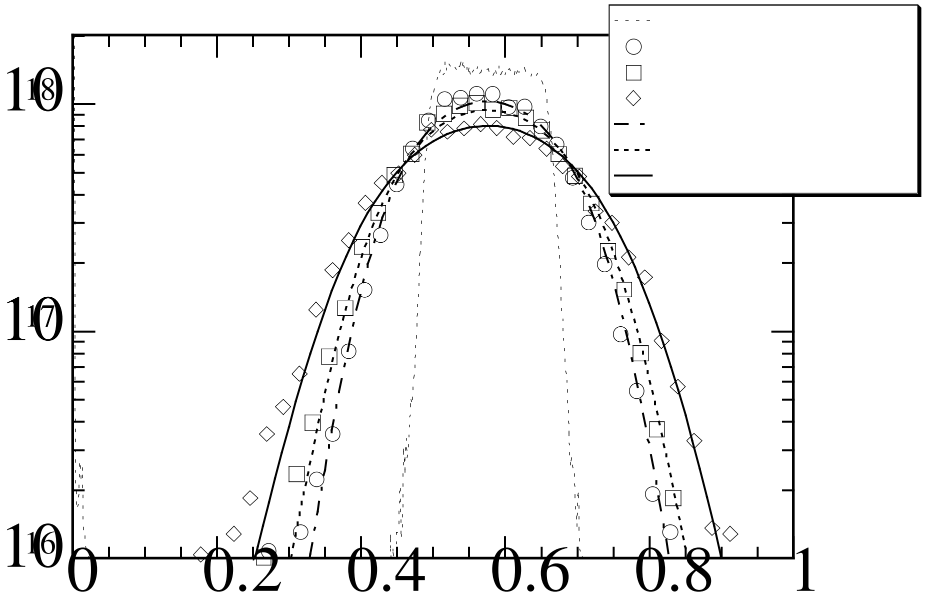

PostScript error

Figure 4.23 Simulation fits to the 2x10^{15} cm^{-2}, 100 keV implanted samples annealed at 750ßC using the scaled +1 approach and the model for dislocation loops. A 7x10^{12} cm^{-2} scaled +1 profile was used. The loops were centered at 0.175 µm, the initial radius of the loops was 10 , the density of the loops was 1.35x10^{10} cm^{-2}, and K_{loop} was 0.35.

the clusters would largely be controlled by the kinetics of the dislocation array which itself could affect not only the equilibrium interstitial concentration, but also the reaction constant for cluster growth and the local interstitial concentration [87]. If this is truly the case, then the simple dislocation loop model accounts for the net effect of the dislocation array on the local interstitial concentration.

4.6.3.4 Comparison of Dissolution Model to Cowern s Cluster Model

Cowern has recently proposed a model to account for cluster dissolution [82],[86]. In this section Cowern s model is compared to our dislocation loop model used to simulate the long-time transient in enhanced boron diffusion.

In Cowern s model the clustered interstitial concentration is added as another solution variable. An initial concentration of clusters must be specified as an input parameter. In this model, as long as clusters exist, the interstitial concentration remains at a steady-state

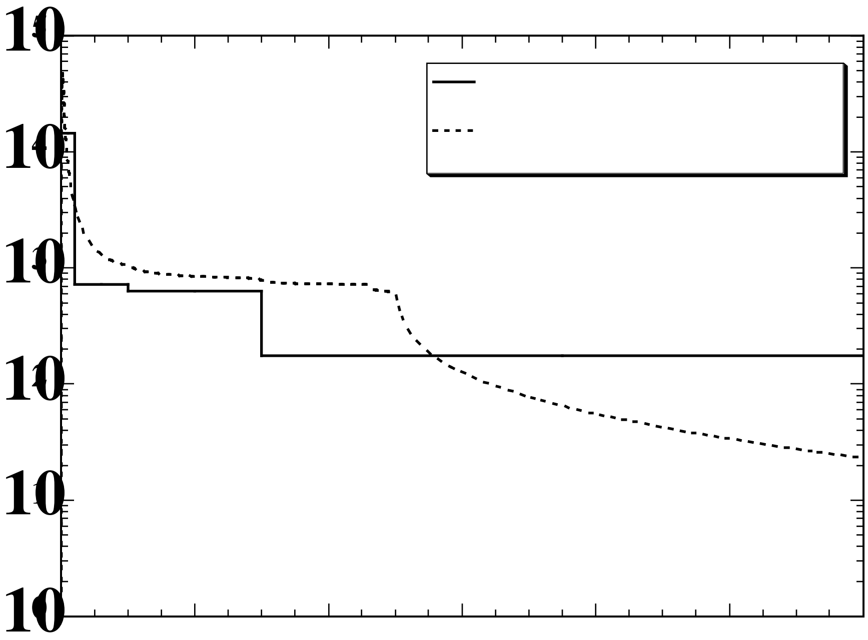

PostScript error

Figure 4.24. Comparison of the time-averaged enhancements in boron diffusivity between time points for the 4x10^{15} cm^{-2}, 50 keV silicon implanted samples annealed at 750ßC for 2, 10, 30, and 120 minutes to the simulated interstitial supersaturation at a depth of 0.6 μm using the scaled +1 approach with the model for loop dissolution. Parameters from Table 4.2 were used in this simulation and a scaled +1 dose of 5x10^{12} cm^{-2} was used as the initial interstitial profile.

value dependent on two reaction rates and the equilibrium interstitial concentration surrounding the clusters (which is a temperature-activated parameter). Once the cluster concentration disappears, the interstitial concentration decays exponentially as a function of time due to an independent interstitial sink that Cowern adds to the interstitial continuity equation (namely, $-R_I(C_I-C_I^*)$). The overall time dependence of the interstitial concentration using Cowern s cluster model is a constant interstitial supersaturation up to a time t_c when the clusters disappear, and then an exponential decay with a single time constant. It has already been shown in Section 4.2 that a single time constant decay cannot describe the experimental data for moderate to high-dose implant damage annealed at 750ßC.

Cowern s model is very similar to our dislocation loop model since in our dislocation loop model, the dissolution rate for very small loops is capped by limiting $C^*_{I,loop}/C_I^*$. This modification can maintain the interstitial concentration at a steady-state value. However, the main difference between Cowern s model and our dislocation loop model is that Cowern only accounts for the clustered interstitial concentration while in the dislocation loop model the actual shrinkage (or growth) of the loops is solved. Thus the dislocation loop model discussed extensively in this thesis is a more kinetic model than Cowern s. One other significant difference in the models is that the exponential decay in the interstitial concentration at long times in Cowern s model is due to the addition of an independent interstitial sink. In the dislocation loop model, no such indepedent sink has been added, and so the long-time transient is governed by point defect diffusion, bulk recombination, and surface recombination resulting in a much more complex time-dependent decay than a simple exponential.

4.7 Summary

In summary, the two.dim and full.cpl diffusion models in SUPREM-IV contain the framework within which the effects of ion implantation damage on dopant diffusion can be modeled. Since the initial point defect profiles right after ion implantation are not well known, we use the simple +1 approach in which each implanted ion will eventually become substitutional creating one free interstitial. Because of the uncertainty in the initial defect profiles, the +1 profile is also scaled up or down by multiplicative constants leading to the scaled +1 approach.

Two models for IED were reviewed and simulation results using these two models were compared to the current experimental data set. Poor agreement between the simulation results and the data was attributed to the fact that the 750ßC data exhibits a two time transition in enhanced diffusion while the simulations predict only one time transition in enhanced diffusion. The scaled +1 approach and the two.dim diffusion model in SUPREM-IV along with one set of activated parameters was shown to fit short-time data for three silicon damage implant conditions annealed between 750ßC and 850ßC.

The long-time transition in the enhanced diffusion for moderate to high-dose implants was attributed to interstitial cluster dissolution which releases excess silicon interstitials. The dislocation loop model described in Chapter 2 was used to mimic cluster dissolution. In order to generate a long-time transient, the equilibrium interstitial concentration surrounding very small loops had to be limited. By limiting the dissolution rate, good agreement between the 750ßC experimental data and the simulations was obtained. Possible physical mechanisms for the limitation on the dissolution rate were discussed, and the dislocation loop model implemented in this work was compared to another recently proposed model for interstitial cluster dissolution.

***FrameMaker has detected one or more
PostScript errors in this document.
()
Please check your output.***